International Journal of Nanomedicine

Dovepress
open access to scientific and medical research

Open Access Full Text Article

ORIGINAL RESEARCH

Administration of Liposomal-Based *Pde3b* Gene Therapy Protects Mice Against Collagen-Induced Rheumatoid Arthritis via Modulating Macrophage Polarization

Longmin Chen[1], Qing Zhou[2], Xun Fang[1], Qianqian Xu[2], Yuan Zou[2], Jing Zhang[2]

[1]Department of Rheumatology and Immunology, the Central Hospital of Wuhan, Tongji Medical College, Huazhong University of Science and Technology, Wuhan, People's Republic of China; [2]Department of Respiratory and Critical Care Medicine, NHC Key Laboratory of Respiratory Disease, Tongji Hospital, Tongji Medical College, Huazhong University of Science and Technology, Wuhan, People's Republic of China

Correspondence: Jing Zhang, Department of Respiratory and Critical Care Medicine, NHC Key Laboratory of Respiratory Disease, Tongji Hospital Research Building, Tongji Hospital, Tongji Medical College, Huazhong University of Science and Technology, Wuhan, Caidian, 430100, People's Republic of China, Email jingzhang@tjh.tjmu.edu.cn

Background: Rheumatoid arthritis (RA) is a chronic and systemic autoimmune disease characterized by synovial inflammation and joint destruction. Despite progress in RA therapy, it remains difficult to achieve long-term remission in RA patients. Phosphodiesterase 3B (Pde3b) is a member of the phosphohydrolyase family that are involved in many signal transduction pathways. However, its role in RA is yet to be fully addressed.

Methods: Studies were conducted in arthritic DBA/1 mice, a suitable mouse strain for collagen-induced rheumatoid arthritis (CIA), to dissect the role of Pde3b in RA pathogenesis. Next, RNAi-based therapy with *Pde3b* siRNA-loaded liposomes was assessed in a CIA model. To study the mechanism involved, we investigated the effect of *Pde3b* knockdown on macrophage polarization and related signaling pathway.

Results: We demonstrated that mice with CIA exhibited upregulated Pde3b expression in macrophages. Notably, intravenous administration of liposomes loaded with *Pde3b* siRNA promoted the macrophage anti-inflammatory program and alleviated CIA in mice, as indicated by the reduced inflammatory response, synoviocyte infiltration, and bone and cartilage erosion. Mechanistic study revealed that depletion of *Pde3b* increased cAMP levels, by which it enhanced PKA-CREB-C/EBPβ pathway to transcribe the expression of anti-inflammatory program-related genes.

Conclusion: Our results support that Pde3b is involved in the pathogenesis of RA, and *Pde3b* siRNA-loaded liposomes might serve as a promising therapeutic approach against RA.

Keywords: rheumatoid arthritis, Pde3b, liposomes, macrophages

Introduction

Rheumatoid arthritis (RA) is a chronic autoimmune inflammatory disease affecting ~0.5–1.0% of the population worldwide.[1] RA is characterized by articular inflammation, often with accumulating joint damage and irreversible disability if insufficiently treated. Currently, RA is still regarded as an incurable disease, and glucocorticoids (GCs), non-steroidal anti-inflammatory drugs (NSAIDs), and disease-modifying anti-rheumatic drugs (DMARDs) are the most commonly used medications in clinic.[2] Although they could relieve symptoms and delay arthritis progression, frequent administration and high dosage are often needed to achieve optimal disease control, which inevitably result in poor compliance and untoward adverse effects.[2,3] Over the past two decades, we have witnessed the evolution and approval of a variety of biological agents, ie, antibodies against tumor necrosis factor (TNF) and interleukin (IL)-6 receptor.

Received: 11 December 2023
Accepted: 9 May 2024
Published: 17 May 2024

However, biologic agents are expensive, and approximately 30–40% of patients do not respond well, accompanied with increased risk of infections.[4,5] Thus, novel therapeutic strategies for RA are urgently needed.

The pathogenesis of RA involves a broad range of inflammatory processes, including dysregulated cytokine production and complicated crosstalk among inflammatory cells.[6] Among these cells, macrophages play a crucial role in shifting synovial inflammation towards a pathological state versus an adaptive response. Macrophages are classified into two subtypes, classically activated macrophages (pro-inflammatory macrophages) and alternatively activated macrophages (anti-inflammatory macrophages).[7,8] In the healthy joint, macrophages typically express anti-inflammatory markers, including arginase 1 (Arg1) and the mannose receptor CD206, and produce immune-regulatory cytokines such as IL-10, IL-13, and transforming growth factor (TGF)-β, which contribute to the maintenance of tissue homeostasis. During RA, however, pro-inflammatory macrophages that secret inflammatory mediators such as IL-1β, IL-6, and TNF-α accumulate in the swollen inflamed synovial tissue and promote tissue destruction and bone erosion.[9] In this respect, shifting synovial macrophages toward anti-inflammatory subtype could be a promising strategy for RA therapy. On the basis of their origins and functions, synovial macrophages can also be divided into tissue-resident and tissue-infiltrating macrophages. Tissue-resident macrophages are predominantly derived from embryonic precursors and to less extent from intermediates of circulating monocytes. They are mainly present in healthy synovium to maintain or restore tissue homeostasis, and those embryo-derived macrophages can sustain replenishment through self-renewal in adulthood.[10] By contrast, tissue-infiltrating macrophages are the key cellular component in synovitis. This population likely originate from circulating monocytes attracted to the synovium by chemokines, where they differentiate into pro-inflammatory macrophages to drive the pathology. Indeed, research has now provided evidence of accelerated monocytopoiesis, their egress from bone marrow, and recruitment into inflamed joints.[11] The rapid development of single cell RNA-sequencing technology has brought unprecedented insights into macrophage heterogeneity within the synovial tissue, uncovering a complete atlas of discrete phenotypic clusters among synovial macrophages. There are two main macrophage populations within the human synovium, $MerTK^{+}CD206^{+}$ tissue-resident macrophages and $MerTK^{-}CD206^{-}$ tissue-infiltrating macrophages.[12] Tissue-resident macrophages contain a $TREM2^{+}CX3CR1^{+}FOLR2^{+}$ cluster and a $LYVE1^{+}$-$FOLR2^{hi}$ cluster. Like resident macrophages, three distinct subpopulations of tissue-infiltrating macrophages have been identified, including a $CD48^{+}S100A12^{+}$ cluster, a $CD48^{+}SPP1^{+}$ cluster (equivalent to mouse $CCR2^{+}IL\text{-}1\beta^{+}$ cluster), and a $CD48^{+}ISG15^{+}$ cluster with an interferon signature (equivalent to mouse $CCR2^{+}ARG1^{+}$ cluster).[13] Additionally, a study published in 2019 identified a population of $CX3CR1^{+}$ tissue-resident macrophages, which control the onset of inflammation via providing a tight junction-mediated protective barrier for intra-articular structures.[14]

Phosphodiesterase 3B (Pde3b) is a cyclic nucleotide phosphodiesterase with a dual-specificity for the second messengers cAMP and cGMP, which are key regulators of many important physiological processes.[15] Although the catalytic domain of Pde3b shows high affinity for both cAMP and cGMP, the velocity for cAMP hydrolysis is 4–10 fold higher than that for cGMP.[16] Pde3b is relatively highly expressed in cells important for the regulation of energy homeostasis, such as hepatocytes, adipocytes, hypothalamic cells, and pancreatic β cells. Therefore, blockade of Pde3b using inhibitor or gene targeting approaches leads to multiple alterations in glucose and lipid metabolism.[17] Recently, an increased Pde3b expression at both mRNA and protein levels was detected in synovial tissue from RA patients and rats.[18] Moreover, diosgenin could inhibit the proliferation, migration, and inflammatory response of RA synovial cells by downregulating Pde3b.[19] This suggests that Pde3b may play an important role in the development of RA, which remains largely unexplored.

The efficient delivery of small interfering RNA (siRNA) to macrophages paves the way to translate the vast knowledge base gained from germline inactivation of genes involved in inflammation to the clinic.[20,21] Among available siRNA delivery systems, cationic liposome is one of the most flexible and successful approaches due to efficient RNA encapsulation, enhanced stability, excellent biocompatibility, and remarkable transfection and targeting efficiencies.[22] Previous studies including ours have proven that liposomes are feasible strategies for RNA interference (RNAi)-based therapy in a variety of disease.[23–25] In addition, genetically engineered nanoparticles were also found to display good performance in RA therapy.[26–28] Thus, we tried to employ *Pde3b* siRNA-loaded liposomes to regulate macrophage polarization for the treatment of RA in the current study. Our results demonstrated that Pde3b was highly expressed in macrophages in the synovial tissue derived from mice with collagen-induced rheumatoid arthritis (CIA). *Pde3b*

knockdown led to decreased cAMP hydrolysis, by which it modulated PKA-CREB-C/EBPβ signaling to promote macrophage anti-inflammatory program. As a result, administration of *Pde3b* siRNA-loaded liposomes significantly alleviated synovial inflammation and bone erosion, along with a higher proportion of anti-inflammatory macrophages both in synovial tissue and draining lymph nodes.

Materials and Methods

Mice

DBA/1 mice were purchased from GemPharmatech Co. (Nanjing, China). Mice were housed in a specific pathogen-free (SPF) facility under a 12-h light/dark cycle with ad libitum access to food and water at 20–24 °C. All animal experiments were performed in accordance with the National Institutes of Health (NIH) guidelines and the proposal approved by the Institutional Animal Care and Use Committee of Huazhong University of Science and Technology ([2022] IACUC Number: 3561).

The collagen-induced rheumatoid arthritis (CIA) mouse model was established by double immunization of 8-week-old male DBA/1 mice. Briefly, 2 mg/mL bovine type II Collagen (CII) was emulsified with complete freund's adjuvant (CFA) at a ratio of 1:1. Mice were primarily immunized with 100μL emulsion of CII/CFA subcutaneously into the base of the tail on day 0, followed by a booster immunization on day 21. Paw thickness was monitored during the experiment, and clinical score was assessed for each mouse for severity of arthritis as previously reported.[29] All mice were euthanized by CO_2 inhalation at day 37 for further histological and flow cytometry analyses.

Histological and Immunofluorescence Analysis

Ankle joints were fixed with 4% paraformaldehyde, decalcified with 0.5 M EDTA for 2 weeks, embedded in paraffin, and then sliced into 5-μm sections. The sections were subjected to hematoxylin and eosin (H&E), safranin O (SO), and toluidine blue (TB) staining as previously described.[30] For immunofluorescence staining, the sections were probed with primary antibodies against F4/80 (sc-377009; Santa Cruz Biotechnology, Santa Cruz, CA, USA) and Pde3b (abs134457, Absin, Shanghai, China).

Flow Cytometry

Single-cell suspension was prepared from mouse popliteal lymph nodes and synovial tissues or retrieved from cell cultures. Cell surface antigens were stained for 30 min on ice with an antibody staining mix diluted in PBS containing 1% BSA. Intracellular staining was performed using the Transcription Factor Buffer Set (562574; BD Biosciences, San Diego, CA, USA) according to the manufacturers' instructions. The following antibodies were used for the studies: PE anti-mouse F4/80 (123110), Brilliant Violet 421 anti-mouse F4/80 (123131), PE/Cy7 anti-mouse CD45 (157205), PE/Cy7 anti-mouse CD206 (141720), PE/Cy7 anti-mouse CD86 (105014), Brilliant Violet 421 anti-mouse CD86 (105031), FITC anti-mouse CX3CR1 (149019), 7-AAD viability staining solution (420403), and PE/Cy7 rat IgG2a, κ isotype ctrl antibody (400521) from Biolegend (San Diego, CA, USA); and PerCP-Cy5.5 rat anti-CD11b (550993) from BD Biosciences (San Diego, CA, USA). Cytometry data were acquired on an Attune NxT (Thermo Fisher Scientific) and analyzed using the FlowJo software version 10. Gating strategies are provided in Supplementary Figure 1.

Generation and Treatment of Bone Marrow-Derived Macrophages (BMDMs)

Bone marrow were flushed from mouse tibias and femurs and meshed through a 70-μm strainer with a syringe plunger. Erythrocytes were lysed with ACK lysis buffer (C3702-120mL; Beyotime, Shanghai, China), then bone marrow cell were resuspended and cultured in RPMI 1640 complete medium (RPMI 1640 with 1% penicillin/streptomycin and 10% FBS) in the presence of 30 ng/mL macrophage colony-stimulating factor (M-CSF, 576406; Biolegend). On day 3 and day 5, the medium was changed with fresh medium containing 20 ng/mL M-CSF, and non-adherent cells were discarded. After a total of 7 days of culture, the differentiated BMDMs were treated with either 100 ng/mL LPS (L4130; Sigma-Aldrich, St. Louis, MO) or 10 ng/mL IL-4 (574306; Biolegend) as indicated time.

RT-qPCR and Western Blot Analysis

Total RNA was isolated from the synovial tissues and cultured cells using the established techniques.[31] cDNA was reverse transcribed following the manufacturer's instructions for HiScript 1st Strand cDNA Synthesis Kit (R111-01; Vazyme, Nanjing, China). Hieff qPCR SYBR Green Master Mix (11203ES03; Yeasen, Shanghai, China) was used for real-time quantitative PCR reaction in the CFX Connect Real-Time PCR Detection System (Bio-Rad). Gene expression was normalized to *Actb* transcript levels. Primers used for qPCR are included in Supplementary Table 1.

For Western blot analysis, cells were washed twice with ice-cold PBS and lysed for 30 min on ice in RIPA buffer (Beyotime, Shanghai, China) supplemented with protease inhibitor cocktail (RM02916; Abclonal, Wuhan, China) and phosphatase inhibitor cocktail (G2007-1ML; servicebio, Wuhan, China). Equal amounts of proteins were separated on SDS-PAGE gels and transferred onto PVDF membranes via wet transfer. Non-specific binding was blocked with 5% skim milk, then membranes were probed with primary antibodies at a 1:1000 dilution. The following commercial antibodies were used: antibodies against Arginase 1 (Arg1) (16001-1-AP), beta Actin (66009-1-Ig), CREB1 (12208-1-AP), and phospho-CREB1 (Ser133) (28792-1-AP) purchased from Proteintech (Wuhan, China); antibody against C/EBPβ (A19538) obtained from Abclonal (Wuhan, China); and antibody against Pde3b (abs134457) originated from Absin (Shanghai, China). Following incubation with HRP-conjugated secondary antibodies (1/5000 dilution), signals were visualized using enhanced chemiluminescence reagent (E412-01; Vazyme, Nanjing, China) and were exposed on the GelView 6000Plus machine (BLT Biotechnology Co., Ltd, Guangzhou, China) or to X-ray film. Images were analyzed with the Image J 1.46r software.

Preparation and Characterization of siRNA-Loaded Liposomes

siRNA-loaded liposomes were prepared using the established techniques.[23] Briefly, 1,2-dimyristoyl-rac-glycero-3-methoxypolyethylene glycol-2000 (mPEGDMG), distearoyl phosphatidylcholine (DSPC), cholesterol, and lipidoid were dissolved in ethanol at a molar ratio of 1.5:10:38.5:50. siRNA was dissolved in 10 mM citrated buffer (pH 3), which was then rapidly mixed with the lipid components by vortex. After removing unentrapped siRNA by ultrafiltration centrifugation, the siRNA-loaded liposomes were diluted in PBS and ready for use. siRNA entrapment efficiency was calculated by Ribogreen assay. The morphology of the liposomes was captured using a transmission electron microscope (TEM, JEM-1230; JEOL, Japan). The polydispersity, zeta potential, hydrodynamic diameter, and stability of the liposomes were examined by dynamic light scattering using a Malvern Zetasizer Nano ZS (UK).

Bone Assessment and Micro-CT Analysis

The ankle joints collected at day 37 following collagen induction were fixed in 4% paraformaldehyde and scanned by ex vivo micro-computed tomography (micro-CT, Skyscan 1276; Bruker, Belgium). Reconstruction was performed to get the 3D images of the joints. Histomorphometric parameters were also analyzed using the CTan1.20.8.0 software.

Assessment of Cardiac, Liver, and Renal Function

Heart function, liver function, and renal function were access by measuring serum creatine kinase (Creatine kinase Assay Kit, A032-1-1), lactate dehydrogenase (Lactate dehydrogenase Assay Kit, A020-2-2), alanine aminotransferase (Alanine aminotransferase Assay Kit, C009-2-1), aspartate aminotransferase (Aspartate aminotransferase Assay Kit, C010-2-1), and creatinine (Creatinine Assay Kit, C011-2-1) using the commercial kits obtained from Nanjing Jiancheng Bioengineering Institute (Nanjing, China).

Seahorse Assay

The oxygen-consumption rate (OCR) was determined on a Seahorse XFe24 analyzer (Agilent Technologies, Santa Clara, CA, USA) as previously described.[31] In brief, BMDMs were seeded at 1×10^5 cells per well in an XF24 culture microplate and treated with IL-4 for 24 h. After washing with the unbuffered XF assay medium, cells were pre-equilibrated in a CO_2-free incubator for 1 h. OCR was then measured in basal condition and upon the sequential addition of 1.5 μM oligomycin, 1.5 μM FCCP, and 0.5 μM antimycin A/rotenone (all from Sigma-Aldrich, St. Louis,

MO). All tests were conducted with 3 replicates per condition, and OCR values of each well were normalized to protein concentration. The results were analyzed with the XFe Wave software (Agilent Technologies).

RNA Sequencing (RNA-Seq) and Bioinformatics Analysis

After IL-4 stimulation for 6 h, total cellular RNA of BMDMs was extracted and subjected to commercial RNA-seq analysis (HaploX Biotechnology). Sequence reads were mapped to the mm10 reference genome and fragments per kilobase of exon per million mapped fragments (FPKMs) were calculated using the Bowtie2 software. Differentially expressed genes (DEGs) were identified on the basis of log2 (fold change) ≥ 0.5 and p value < 0.05. Heatmaps were drawn with the R package pheatmap. Gene set enrichment analysis (GSEA) was performed using the GSEA package. The RNA-seq data have been deposited in the NCBI public repository Sequence Read Archive (Bioproject ID: PRJNA1025256).

Chromatin Immunoprecipitation (ChIP) Assay

The ChIP assay was performed following the manufacturers' instructions of the ChIP Assay Kit (P2078; Beyotime, Shanghai, China). Briefly, after stimulation with IL-4 for 12 h, BMDMs were crosslinked with 1% formaldehyde for 10 min and quenched with 0.125 M glycine. Lysates were sonicated using the UCD-300 Bioruptor (Diagenode, Denville, NJ, USA) to shear the DNA to an average length of 400–800 bp. The sonicated supernatants were then incubated with Protein A/G agarose beads immobilized with anti-C/EBPβ or rabbit IgG control (30000-0-AP; Proteintech, Wuhan, China) overnight at 4 °C under gentle rotation. After extensive washes, immunocomplexes were eluted with elution buffer (1% SDS and 0.1 M $NaHCO_3$) and incubated with 0.2 M NaCl at 65 °C for 4 h to reverse the crosslinks. DNA was purified using a DNA Purification Kit (D0033; Beyotime, Shanghai, China) and subjected to qPCR analysis. The data were normalized to the input. The primers used for the ChIP assay are listed in Supplementary Table 2.

RNAi Transfection

siRNA targeting mouse *Pde3b* was purchased from Ribobio (Guangzhou, China), and scramble siRNA that does not match any sequence in the mouse genome was also provided by the manufacturer and used as a negative control. BMDMs were transfected with siRNAs using the Lipofectamin 3000 (L3000015; Invitrogen, Carlsbad, CA) in Opti-MEM reduced serum media (31985070; Gibco). The culture medium was changed 18 h later, and the cells were cultured for another 24 h before subsequent experiments. Targeted siRNA sequences were as follows: si-*Pde3b*-01: 5′-GCCAAGGCCAATGATGTAA-3′, si-*Pde3b*-02: 5′-CCTGTGCAACTCCTATGAT-3′, and si-*Pde3b*-03: 5′-CTGGACAGATTGCTTACAT-3′.

Statistical Analysis

Data were presented as mean ± SEM. Exact numbers of replicates are indicated in the figure legends. Statistical analysis was performed using the GraphPad Prism software version 6.01 (GraphPad Software Inc., San Diego, CA). The differences between groups were accessed by unpaired Student's t test (comparison of two groups) or one-way ANOVA (more than two groups) where applicable. For all statistical comparisons, p values of less than 0.05 were considered as statistically significant.

Results

RA is Characterized by Altered Pde3b Expression in Macrophages

To address the role of Pde3b in RA, we developed CIA model in DBA/1 mice and collected ankle joints for immunofluorescence staining. Pde3b was almost undetectable in the synovial tissue from control mice, while RA mice-derived joint sections were characterized by a large amount of synovial macrophage aggregation, manifesting high Pde3b expression level evidenced by the co-localization of Pde3b and F4/80 (Figure 1). These results suggest that Pde3b is overexpressed in macrophages during the pathogenesis of RA.

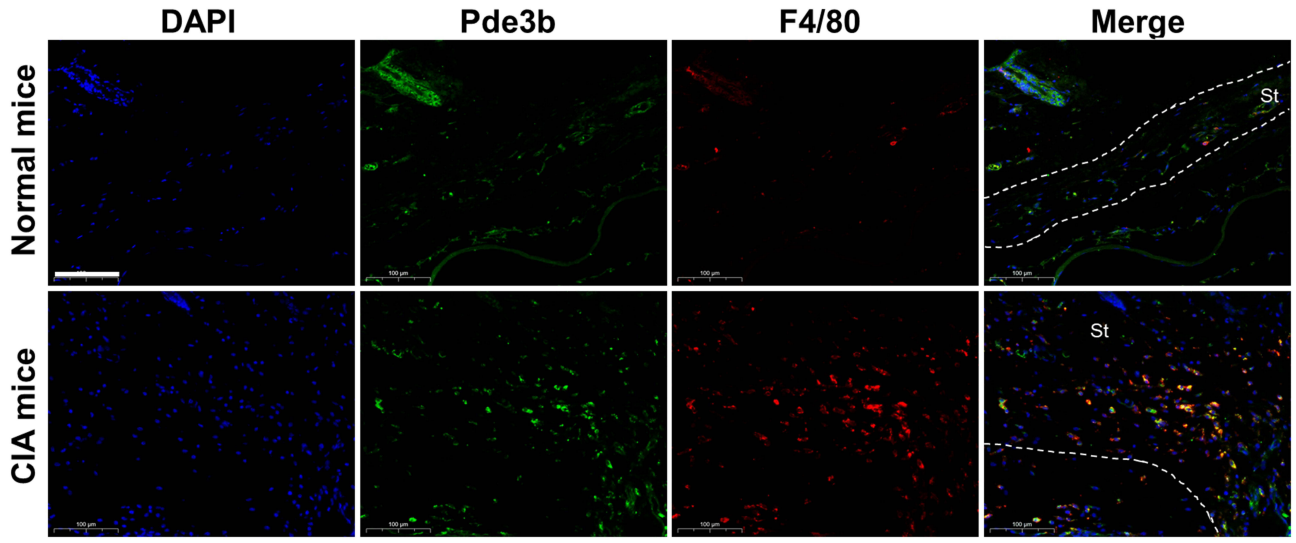

Figure 1 Arthritic mice exhibit increased Pde3b expression in synovial macrophages. Representative immunofluorescence staining results for F4/80 and Pde3b in joint sections from controls and arthritic mice. Scale bars: 100 μm. Original magnification: ×400. St, synovial tissue.

Silencing *Pde3b* Promotes an Anti-Inflammatory Macrophage Program

To explore the effect of Pde3b on macrophages, we design three *Pde3b* siRNA and transfected BMDMs. RT-qPCR and Western blot analyses indicated that *Pde3b* siRNA-3 had the highest interference efficiency (Figure 2a and b), which was selected for subsequent experiments. Next, we conducted deep RNA sequencing using BMDMs transfected with scramble or *Pde3b* siRNA after IL-4 stimulation. The *Pde3b* siRNA-transfected BMDMs were characterized by 366 upregulated and 546 downregulated genes as compared with control BMDMs (Figure 2c). Among the top 10 upregulated genes, anti-inflammatory program-related genes were noted, including *Arg1* and *Retnla* (Figure 2d), which was further confirmed by RT-qPCR and Western blot analyses (Figure 2e and f). Indeed, BMDMs transfected with *Pde3b* siRNA had an increase in CD206 expression in response to IL-4 stimulation, although no perceptible difference of CD206 expression was observed before IL-4 treatment (Figure 2g). Moreover, the activation marker CD86 was reduced in *Pde3b* siRNA-transfected BMDMs upon stimulation with LPS (Figure 2h), along with decreased production of proinflammatory cytokines TNF-α, IL-6, and IL-1β (Figure 2i).

Interestingly, GSEA Pre-ranked analysis of RNA-seq data noted upregulated tricarboxylic acid (TCA) cycle in *Pde3b* siRNA-transfected BMDMs (Figure 2j). Therefore, we conducted metabolic assay and monitored oxygen-consumption rate (OCR) to determine the mitochondrial respiration. The *Pde3b* siRNA-transfected BMDMs exhibited higher basal OCR coupled with increased spare respiratory capacity (SRC) following IL-4 induction (Figure 2k and l), suggesting that the *Pde3b* siRNA-transfected BMDMs were featured with the increased commitment to oxidative phosphorylation (OXPHOS), which favors anti-inflammatory macrophage polarization.[31] Overall, these data support that *Pde3b* knock-down selectively orchestrates macrophage anti-inflammatory program.

Preparation and Characterization of *Pde3b* siRNA-Loaded Liposomes

To translate our findings into a therapeutic approach against RA, we prepared cationic liposomes carrying *Pde3b* siRNA (Figure 3a) and checked their characteristics. The generated liposomes manifested >95% entrapment efficiency for loading siRNA with a polymer dispersity index (PDI) of 0.15 (Figure 3b). The zeta-potential of siRNA-loaded liposomes was decreased (2.7 mV at 25°C) as compared with that of blank liposomes (10.3 mV at 25°C) because of the electronegative nature of siRNA. As shown in the TEM image, the liposomes manifested a uniform sphere morphology (Figure 3c). In addition, these liposomes displayed a normal distribution of hydrodynamic diameter (Figure 3d) and could maintain stability for at least 24 hours (Figure 3e).

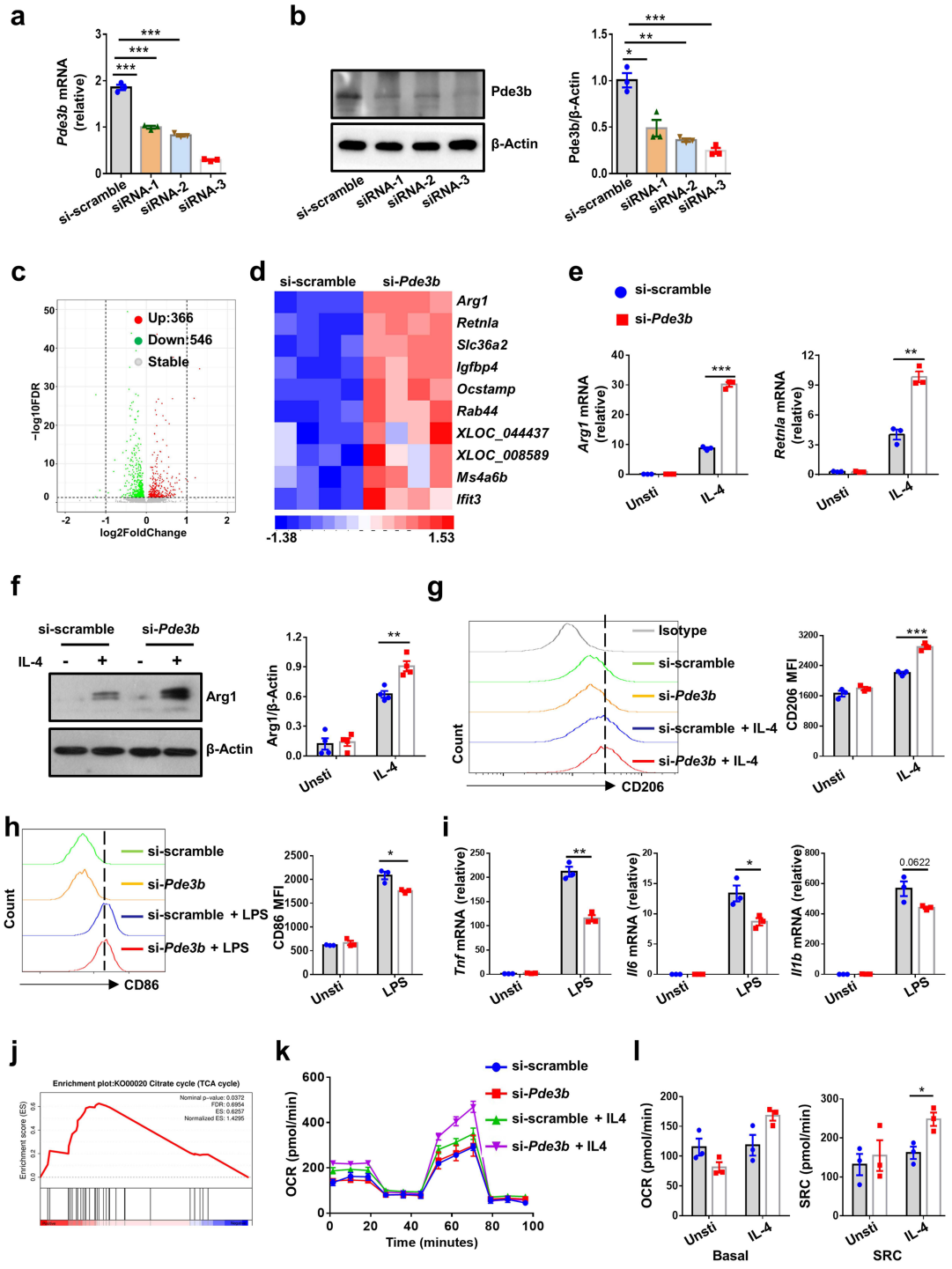

Figure 2 *Pde3b* knockdown orchestrates alternative activation of macrophages. (**a** and **b**) Verification of the interference efficiency of *Pde3b* siRNAs in BMDMs at the mRNA (**a**) and protein (**b**) level. (**c**) Volcano plot of the differentially expressed genes (DEGs) between scramble and *Pde3b* siRNA-transfected BMDMs, as determined by RNA-seq. Four biological replicates were included for each group. (**d**) Heatmap showing the top 10 significantly upregulated genes in *Pde3b* siRNA-transfected BMDMs. (**e**) RT-qPCR analysis of *Arg1* and *Retnla* mRNA expression in scramble and *Pde3b* siRNA-transfected BMDMs, either unstimulated or treated with IL-4 for 6 h. (**f**) Western blot analysis of Arg1 expression in BMDMs before and after IL-4 stimulation. (**g**) Representative FACS plots and quantitative data of CD206 expression in BMDMs with or without IL-4 stimulation for 24 h. (**h**) Flow cytometry analysis of CD86 expression in scramble and *Pde3b* siRNA-transfected BMDMs with or without LPS treatment for 24 h. (**i**) RT-qPCR analysis of relative mRNA levels of *Tnf, Il6* and *Il1b* in BMDMs treated with or without LPS. (**j**) Gene set enrichment of genes describing for TCA cycle in *Pde3b* siRNA-transfected BMDMs, relative to scramble siRNA-transfected BMDMs. (**k**) OCR of scramble and *Pde3b* siRNA-transfected BMDMs with or without IL-4 stimulation for 24 h, which was assessed before and after sequential addition of oligomycin, FCCP, and antimycin A/rotenone. (**l**) Accordingly, basal OCR and spare respiratory capacity (SRC) were shown. Data were collected from three (a, b, e, g-i, k, and l) or four (f) independent experiments. Values are presented as mean ± SEM. Significance was determined by one-way ANOVA in (**a** and **b**) and by unpaired Student's *t* test in other figure parts. **p* < 0.05; ***p* < 0.01; ****p* < 0.001. Arg1, Arginase 1; Unsti, unstimulated.

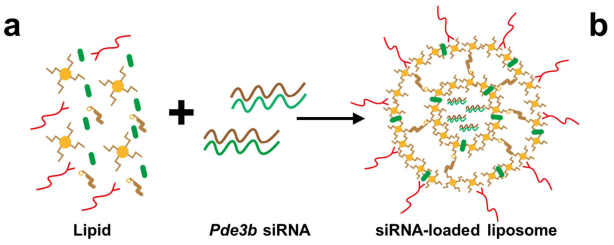

b

	Blank liposome	siRNA loaded liposome
Hydrodynamic diameter (nm)	123	101
PDI	0.18	0.15
Zeta-potentical (mv)	10.3	2.7
Entrapment effiency (%)	/	>95

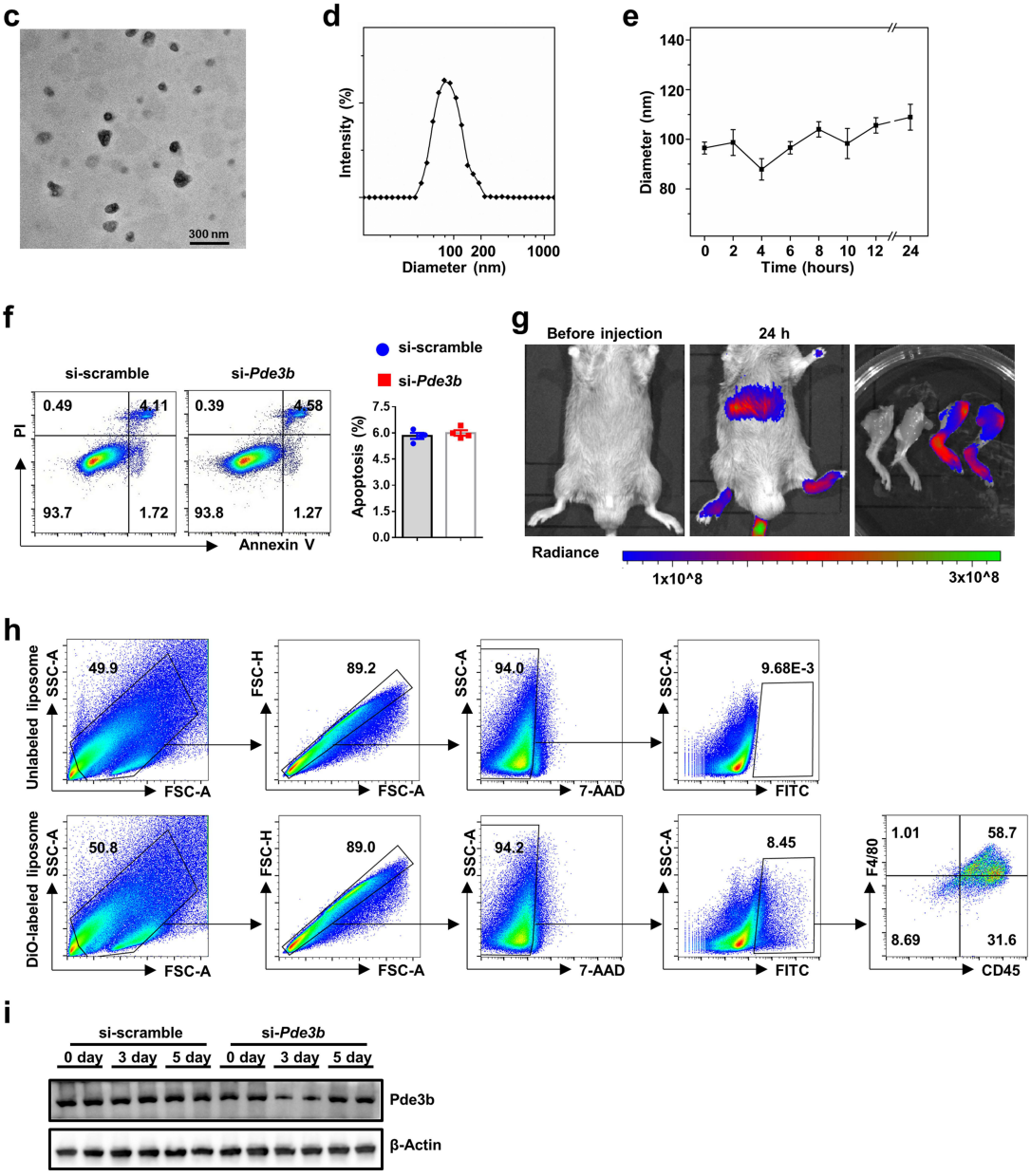

Figure 3 Characterization and biodistribution of the siRNA-loaded liposomes. (**a**) Schematic diagram showing generation of the *Pde3b* siRNA-loaded liposomes. (**b**) Hydrodynamic diameter, polymer dispersity index (PDI), and zeta-potential of blank and siRNA-loaded liposomes measured by dynamic light scattering (DLS). siRNA entrapment efficiency was evaluated by Ribogreen assay. (**c**) Representative transmission electron microscopy (TEM) image of siRNA-loaded liposomes. Scale bars: 300 nm. (**d**) Hydrodynamic diameter distribution of siRNA-loaded liposomes. (**e**) Colloid stability of siRNA-loaded liposomes in PBS solution. (**f**) The biosafety of siRNA-loaded liposomes in vitro determined by flow cytometry. (**g**) Ex vivo DiR fluorescence images showing the biodistribution of siRNA-loaded liposomes in arthritic mice at 24 h post injection. (**h**) Flow cytometry analysis of the DiO-labeled liposome distribution in the ankle joints of arthritic mice. (**i**) Temporal expression of Pde3b in synovial tissues after administration of the scramble siRNA- or *Pde3b* siRNA-loaded liposomes. Data are expressed as mean ± SEM. Statistical difference in (**f**) was analyzed using unpaired Student's *t* test.

We then used flow cytometry to examine the impact of siRNA-loaded liposomes on BMDM viability. BMDMs treated with siRNA-loaded liposomes retained more than 90% viability after 24 h (Figure 3f), hinting that they had good in vitro biocompatibility. To evaluate the in vivo behavior, lipophilic carbocyanine DiOC18 (DiR)-labeled liposomes were intravenously administrated to mice with CIA, and the fluorescent signal was tracked using an In Vivo Imaging System (IVIS). As expected, there was a strong liposome accumulation in the flamed joints of RA mice, which remained high 24 h after injection (Figure 3g). Next, the distribution of liposomes in the inflamed joints was further investigated. Flow cytometry results showed that liposomes mainly overlapped with $F4/80^+$ macrophages (Figure 3h), suggesting a high efficiency for their uptake by macrophages. Finally, we assessed the temporal expression of Pde3b after delivery of siRNA-loaded liposomes to clarify the optimal time interval for the treatment. A significant decline in Pde3b expression was detected at day 3 after liposome administration, which returned to normal level at day 5 (Figure 3i). Taken these data together, our results support that the liposomes predominantly accumulated in the flamed joint of RA mice, particularly in macrophages, which makes it a promising therapeutic strategy for RA.

Administration of *Pde3b* siRNA-Loaded Liposomes Protects Mice Against CIA

Given that RA mice showed enhanced expression of Pde3b in macrophages, we then examined the therapeutic effect of *Pde3b* siRNA-loaded liposomes on RA. We generated CIA mouse model, and intravenously injected liposomes, *Pde3b* siRNA (using the same siRNA amounts as the latter two groups), scramble siRNA-loaded liposomes, or *Pde3b* siRNA-loaded liposomes every 4 days from day 17 (Figure 4a). The *Pde3b* siRNA-loaded liposomes-treated mice developed less severe arthritis as compared to that of other groups of mice, as evidenced by the ameliorated hind paw swelling (Figure 4b and c) and lower clinical score (Figure 4d). To further assessed synovial inflammation and soft tissue disorder, the ankle joints of mice were sectioned at the study endpoint, and stained with hematoxylin and eosin (H&E), toluidine blue (TB) and safranin O (SO). Histopathological analysis revealed less severe synovial hyperplasia and a huge drop in inflammatory cell infiltration, accompanied by reduced bone and cartilage destruction in the *Pde3b* siRNA-loaded liposomes-treated mice (Figure 4e). In consistent with those observations, the *Pde3b* siRNA-loaded liposomes-treated mice showed a significant lower level of serum proinflammatory cytokines including IL-1β (Figure 4f), TNF-α (Figure 4g), and IL-17A (Figure 4h).

Next, micro-CT was used to verify the situation of bone destruction. The ankle joint of mice in the CIA control group manifested rough bone surface and serious bone erosion (Figure 5a and b), as well as a marked reduction of BMD (bone mineral density) (Figure 5c) and an increase of BS/BV (bone surface vs bone volume) (Figure 5d) compared with the normal group. Strikingly, treatment with *Pde3b* siRNA-loaded liposomes resulted in an obvious improvement of bone surface and BMD. The trabecular parameters also confirmed that *Pde3b* siRNA-loaded liposome treatment could potently increase the trabecular number (Tb.N) and trabecular bone thickness (Tb.Th) while decrease trabecular separation (Tb.Sp) (Figure 5e-g), implying evident inhibition of erosive bone damage. Overall, these results suggest that *Pde3b* siRNA-loaded liposomes could attenuate CIA with high efficacy.

To evaluate the potential toxicity of the liposomes, we checked various serum biochemical parameters with particular attention to heart (creatine kinase), liver (lactate dehydrogenase, alanine aminotransferase, and aspartate aminotransferase), and kidney (creatinine). As expected, none of them showed significant changes compared to those of the normal mice (Supplementary Figure 2a). In addition, H&E staining showed no apparent histopathological abnormalities or lesions in the major organs (Supplementary Figure 2b), suggesting that liposome treatment did not have significant toxic effect on mice.

Pde3b Knockdown Promotes Anti-Inflammatory Macrophage Polarization During RA Progression

Since the in vitro experiments supported that *Pde3b* silencing could orchestrate the anti-inflammatory program in macrophages (Figure 2), we further explored whether *Pde3b* siRNA-loaded liposomes would exert similar effects in vivo. To this end, macrophage profiling in the synovial tissues and popliteal lymph nodes following collagen induction was examined by flow cytometry analysis. Indeed, the proportion of $F4/80^+CD11b^+$ cells in the synovial tissues was ~39% lower in the *Pde3b* siRNA-loaded liposomes-treated mice compared to that in scramble siRNA-loaded liposomes-treated mice (Figure 6a),

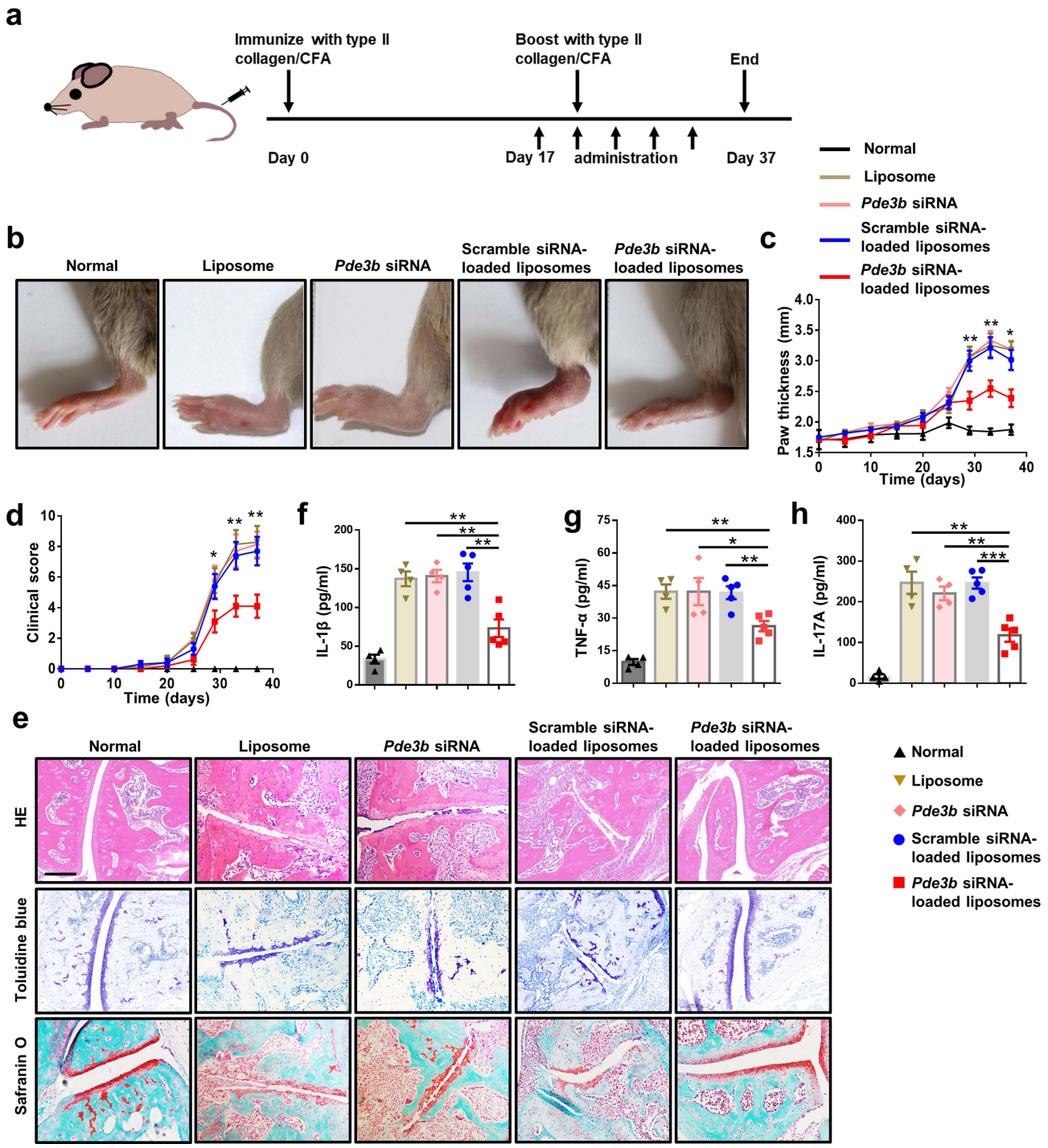

Figure 4 Therapeutic efficacy of the *Pde3b* siRNA-loaded liposomes in mice with collagen-induced arthritis (CIA). (**a**) Schematic outline of the experimental design and time line of liposome treatment. (**b**) Representative image of the hindlimbs at the endpoint of the experiment. (**c**) Paw thickness of CIA mice recorded during the experimental process. (**d**) Graph summarizing clinical score. Normal mice, n = 4; CIA mice treated with blank liposome and *Pde3b* siRNA, n = 7 per group; CIA mice treated with siRNA-loaded liposomes, n = 10 in each study group (**c, d**). (**e**) Representative images for H&E (top), toluidine blue (middle), and safranin O (bottom) staining of ankle joints at the endpoint of the experiment. Scale bars: 200 μm. Original magnification: ×200. (**f-h**) Analysis of plasma IL-1β (**f**), TNF-α (**g**), and IL-17A (**h**) levels in normal mice (n = 4), CIA mice treated with blank liposome (n = 4), *Pde3b* siRNA (n = 4), and siRNA-loaded liposomes (n = 5 per group). Values are expressed as mean ± SEM, and one-way ANOVA was employed for data analysis. **p* < 0.05; ***p* < 0.01; ****p* < 0.001.

indicating dramatically decreased macrophage accumulation. Synovial macrophages from the *Pde3b* siRNA-loaded liposomes-treated mice expressed lower levels of the pro-inflammatory marker CD86 (Figure 6b), while expression of the typical anti-inflammatory surface antigen CD206 was much higher than those from other groups of arthritic mice (Figure 6c). Similar

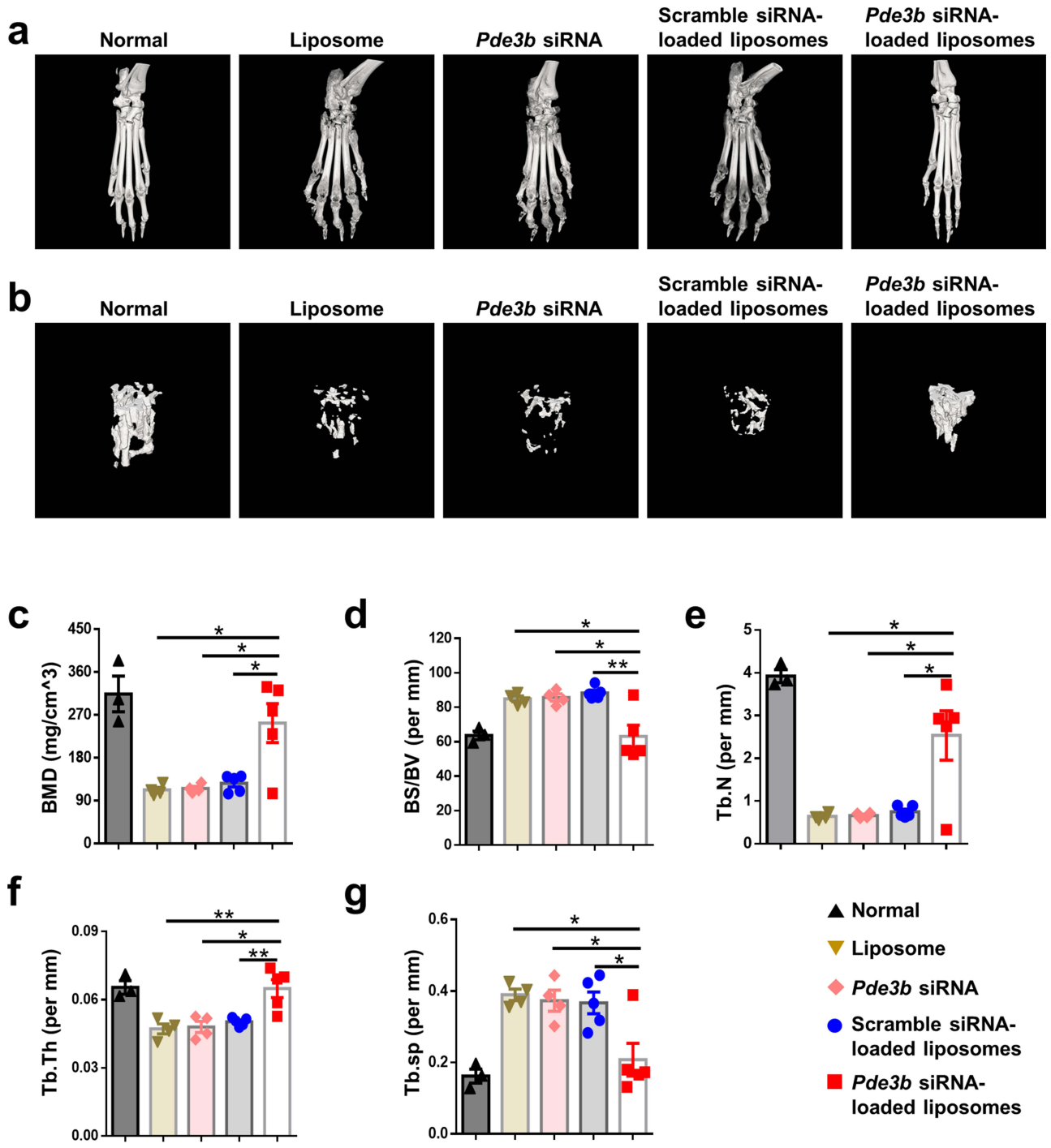

Figure 5 Administration of *Pde3b* siRNA-loaded liposomes prevents bone erosion in arthritic mice. (**a**) Representative 3D-reconstructed images of hind paws by micro-CT analysis. (**b**) Representative micro-CT images of the reconstructed trabecular structure in bone. (**c-g**) Quantitative micro-CT analysis of BMD (**c**), BS/BV (**d**), Tb.N (**e**), Tb.Th (**f**), and Tb.Sp (**g**) of the ankle joints at the endpoint of the experiment. Normal mice, n = 3; CIA mice treated with blank liposome and *Pde3b* siRNA, n = 4 for each group; CIA mice treated with siRNA-loaded liposomes, n = 5 for each group. Values are presented as mean ± SEM. Statistical significance was accessed by one-way ANOVA. *$p < 0.05$; **$p < 0.01$. BMD bone mineral density; BS/BV, bone surface vs bone volume; Tb.N, trabecular number; Tb.Th, trabecular bone thickness; Tb.Sp trabecular separation.

results were noted in the popliteal lymph nodes as well, although there was no significant change in the proportion of macrophages (Figure 6d-f). Given the crucial role of $CX3CR1^+$ resident synovial macrophages in forming a protective barrier for the joint,[14] we analyzed this population in the synovial tissue. However, no perceptible difference was noted between *Pde3b* siRNA-loaded liposomes-treated mice and other groups of mice (Supplementary Figure 3). The expression levels of

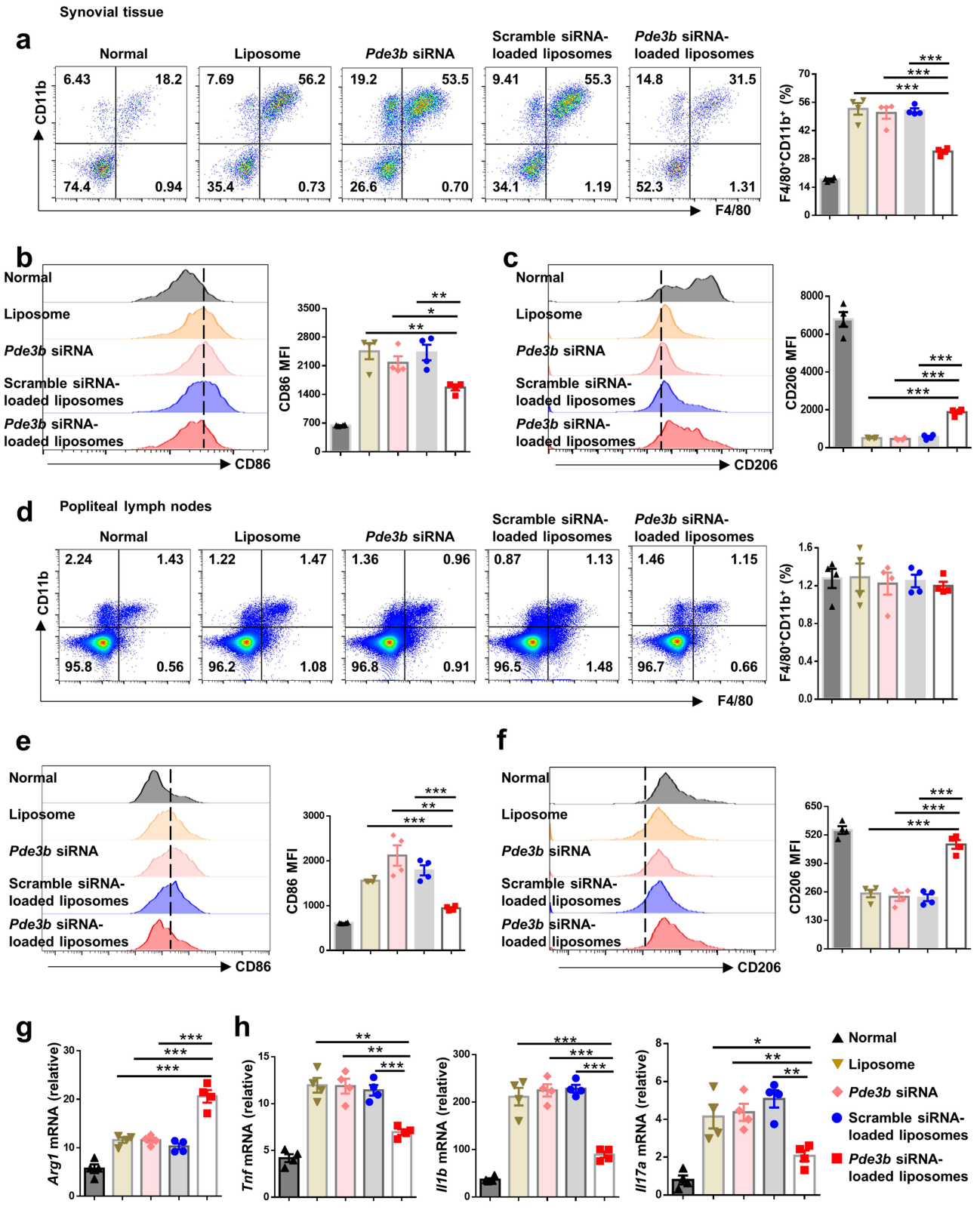

Figure 6 Silencing *Pde3b* promotes anti-inflammatory macrophage polarization in vivo. (**a-f**) Single-cell suspension was prepared from mouse synovial tissues and popliteal lymph nodes at the endpoint of the experiment and subject to flow cytometry analysis. (**a**) Representative FACS plots and percentages of F4/80$^+$CD11b$^+$ macrophages in the synovial tissues from normal mice and CIA mice treated with blank liposome, *Pde3b* siRNA, or siRNA-loaded liposomes. (**b** and **c**) Flow cytometry analysis of CD86 (**b**) and CD206 (**c**) expression in synovial macrophages. (**d**) Representative FACS plots and percentages of F4/80$^+$CD11b$^+$ macrophages in the popliteal lymph nodes from normal mice and CIA mice treated with blank liposome, *Pde3b* siRNA, or siRNA-loaded liposomes. (**e** and **f**) Flow cytometry analysis of CD86 (**e**) and CD206 (**f**) in macrophages from the popliteal lymph nodes. (**g** and **h**) RT-qPCR analysis of the mRNA abundance for the indicated genes in synovial tissues. n = 4 in each study group. Data are presented as mean ± SEM. Statistical difference was determined by one-way ANOVA. *$p < 0.05$; **$p < 0.01$; ***$p < 0.001$.

Arg1 in synovial tissue homogenates were consistently and substantially increased in *Pde3b* siRNA-loaded liposomes-treated mice (Figure 6g). Moreover, injection of *Pde3b* siRNA-loaded liposomes significantly decreased the levels of *Tnf, Il1b*, and *Il17a* (Figure 6h), as illustrated by RT-qPCR analysis. Therefore, liposomes carrying *Pde3b* siRNA efficiently augments anti-inflammatory macrophage polarization during the pathological process of RA.

Knockdown of *Pde3b* Enhances PKA-CREB-C/EBPβ Signaling to Augment Anti-Inflammatory Macrophage Polarization

C/EBPβ is one of the key transcription factors that are clearly associated with anti-inflammatory macrophage polarization,[32] while cAMP stimulates the activity of PKA, which subsequently phosphorylate CREB to transcribe C/EBPβ expression.[33] Therefore, we investigated whether Pde3b modulate anti-inflammatory macrophage polarization through cAMP-PKA-CREB-C/EBPβ signaling. Indeed, the *Pde3b* siRNA-transfected BMDMs displayed significantly higher levels of cAMP in the culture supernatants as compared to that of BMDMs transfected with scramble siRNA (Figure 7a). An increased

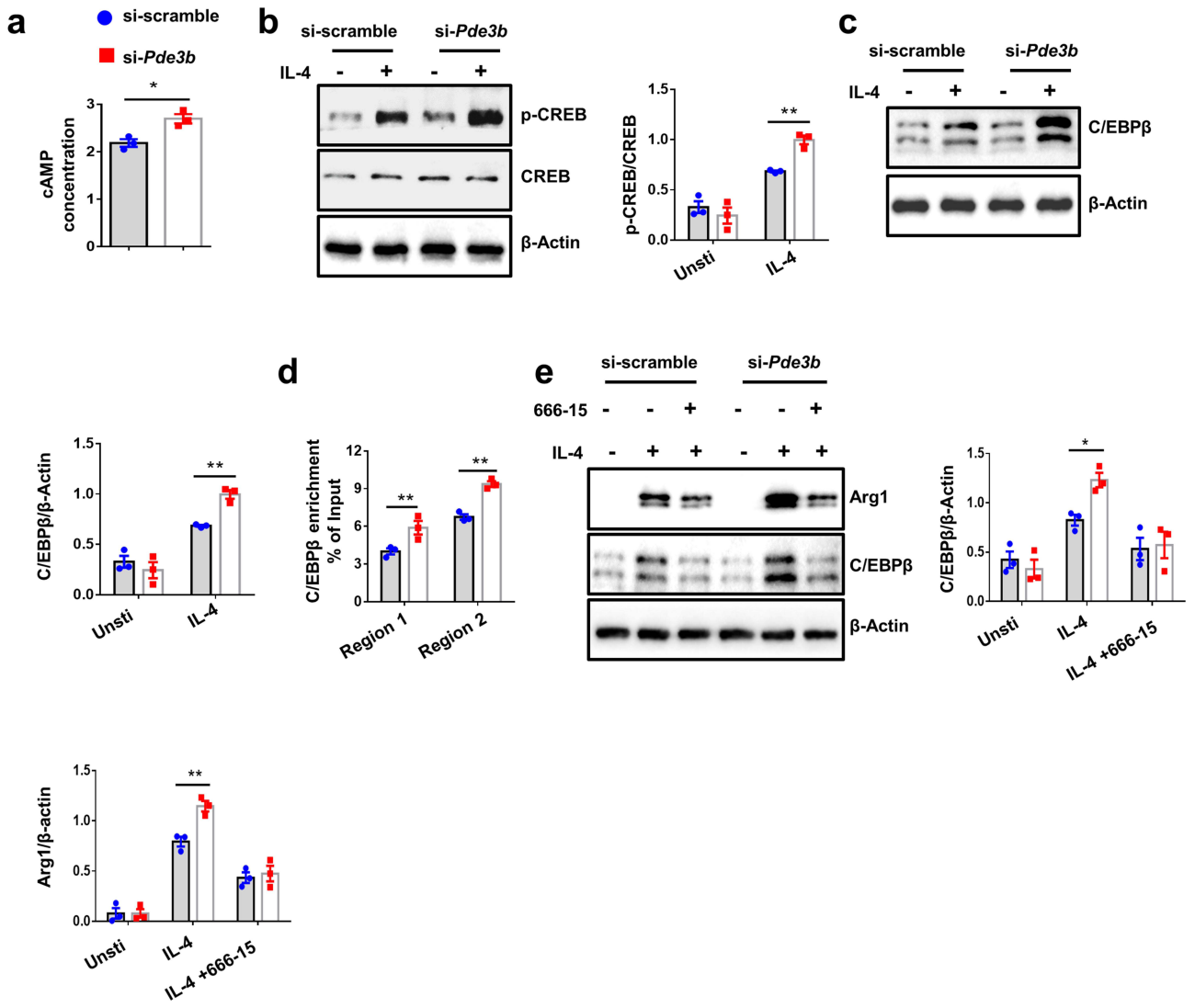

Figure 7 *Pde3b* knockdown enhances macrophage anti-inflammatory program by regulating PKA-CREB-C/EBPβ signaling. (**a**) ELISA analysis of cAMP in the culture supernatants of BMDMs transfected with scramble or *Pde3b* siRNA. (**b**) Western blot analysis of (p-)CREB expression in BMDMs before and after IL-4 stimulation. (**c**) Results for C/EBPβ expression in BMDMs with or without IL-4 stimulation for 24 h. (**d**) ChIP-qPCR was performed for C/EBPβ in the *Arg1* promoter in scramble or *Pde3b* siRNA-transfected BMDMs following IL-4 stimulation. (**e**) Western blot analysis of C/EBPβ and Arg1 levels in scramble or *Pde3b* siRNA-transfected BMDMs under indicated culture conditions. Data were collected from three independent experiments (**a-e**). Values are expressed as mean ± SEM. Statistical significance was analyzed by unpaired Student's *t* test. *$p < 0.05$; **$p < 0.01$. Unsti, unstimulated.

CREB phosphorylation was also noted in *Pde3b*-depleted BMDMs following IL-4 stimulation (Figure 7b), along with markedly elevated levels of C/EBPβ (Figure 7c). Consistently, the binding of C/EBPβ to the promoter regions of anti-inflammatory macrophage-specific gene *Arg1* was increased in BMDMs transfected with *Pde3b* siRNA (Figure 7d).

To further confirm the above results, a rescue experiment was conducted. BMDMs were stimulated with IL-4 in the presence of 666–15, a potent and selective CREB inhibitor. Addition of 666–15 significantly reduced expression of C/EBPβ in the *Pde3b*-depleted BMDMs to a comparative level as the control BMDMs (Figure 7e). Moreover, 666–15 completely abolished the effect of *Pde3b* knockdown on macrophage anti-inflammatory program as evidenced by similar expression level of Arg1 between *Pde3b* and scramble siRNA-transfected BMDMs (Figure 7e). Collectively, these results indicate that *Pde3b* knockdown upregulates cAMP level, by which it enhances PKA-CREB-C/EBPβ signaling to promote macrophage anti-inflammatory program.

Discussion

RA is a common systemic autoimmune disease that primarily affects the joints. Current therapies adequately benefit only approximately 50% of patients; half then relapse after treatment cessation.[12] Therefore, exploration of additional pathogenic factors and development of new therapeutics are urgently needed. In this report, we provide convincing evidence that macrophages originated from mice with collagen-induced arthritis manifest enhanced Pde3b expression. Pde3b catalyze the hydrolysis of cAMP, thereby suppressing PKA-CREB-C/EBPβ signaling to attenuate macrophage anti-inflammatory program. Consistently, administration of liposomes carrying *Pde3b* siRNA significantly promotes the anti-inflammatory-biased macrophage phenotype in the synovial tissues and inhibits synovial inflammation and bone erosion. Together, our results not only demonstrate an essential role of Pde3b in RA pathogenesis, but also suggest that Pde3b could be a viable target against RA in clinical settings.

The superfamily of PDEs comprises 11 subfamilies with different subcellular localization and substrate specificity.[34] Owing to the distinct functional compartmentalization of each PDE isoform and their importance in multiple physiologic processes, PDEs have been served as targets for pharmacological intervention.[35] Pde3b is a member of the PDE superfamily reported to be implicated in the regulation of metabolism in the liver, adipose tissues, and pancreatic β cells.[36] Interestingly, a recent study demonstrated higher levels of Pde3b mRNA and protein in synovial tissues from RA patients,[18] hinting a potential role of Pde3b in RA pathogenesis. To address this hypothesis, we first defined the cell type that caused differential Pde3b level. It was noted that Pde3b was predominantly localized within $F4/80^{+}$ macrophages in joint sections from CIA mice, which promoted us to embark on the effect of Pde3b on macrophages.

Polarization state of synovial macrophages is closely related to disease activity and severity of RA and provides valuable clues for RA treatment.[9] Compelling evidence has demonstrated that classically activated macrophages secrete high levels of proinflammatory cytokines and chemokines, leading to exacerbated symptoms and signs of RA, whereas alternatively activated macrophages restrain inflammatory responses and repair damaged tissues.[37,38] Indeed, reprogramming macrophages toward anti-inflammatory phenotype alleviates synovial inflammation and joint destruction in collagen-induced arthritic mice.[9] In this study, we transfected BMDMs with *Pde3b* siRNA, and then treated with IL-4 to determine the impact of Pde3b on macrophage polarization. Flow cytometry analysis revealed that silencing *Pde3b* robustly facilitated IL-4-induced polarization of anti-inflammatory macrophages, as evidenced by higher expression of CD206. Western blot and RT-qPCR analyses detected significantly increased anti-inflammatory macrophage markers such as Arg1 and Retnla, which further corroborated the facilitated macrophage anti-inflammatory program. It has been reported that pro-inflammatory macrophages have a broken TCA cycle, while anti-inflammatory macrophages maintain an intact TCA cycle and favor oxidative metabolism, especially fatty acid oxidation (FAO), as a mode of ATP production.[31,39] Consistent with this notion, upregulated TCA cycle and increased commitment to oxidative phosphorylation were also observed in *Pde3b*-depleted BMDMs.

The next critical issue is to dissect the molecular mechanism underlying Pde3b regulation of macrophage polarization. As expected, *Pde3b* siRNA-transfected BMDMs exhibited increased cAMP level as compared to that of scramble siRNA-transfected BMDMs after IL-4 stimulation. cAMP transduces signal-encoded information by acting through a number of downstream targets, among which PKA is clearly essential for the development of the Pde-related phenotype.[40,41] Upon activation, PKA is capable of phosphorylating CREB, which regulates the transcription of

numerous genes including C/EBPβ. Considering the critical role of C/EBPβ played in anti-inflammatory macrophage polarization,[42] we checked the effect of Pde3b on PKA/CREB/C/EBPβ signaling in macrophages. Indeed, higher levels of p-CREB and C/EBPβ were detected in the *Pde3b* siRNA-transfected BMDMs. Additionally, the use of a chemical CREB inhibitor almost completely rescued the upregulated anti-inflammatory macrophage signature in *Pde3b*-depleted BMDMs, suggesting that silencing *Pde3b* promotes the macrophage anti-inflammatory program predominantly through PKA/CREB/C/EBPβ signaling, although we cannot completely exclude that additional mechanisms might be implicated.

Given the fact that safe and effective therapeutic options for RA are still limited, numerous clinical trials have been conducted to exploit promising drugs for the treatment of RA. RNAi, a process involved in sequence-specific control of gene expression, is one of the most important and exciting discoveries in the past few decades.[43] siRNAs can trigger RNAi and thus provide a powerful tool to potently and specifically silence a disease-related gene.[43] However, unmodified siRNA as a therapeutic, is challenging because of its short half-life, limited bioavailability, and poor target affinity following systemic administration.[44] Liposomes are established drug carriers with safety and capability to provide controlled drug release, which can entrap a wide range of therapeutic molecules, including siRNA.[23] Meanwhile, the first siRNA-loaded liposome (patisiran) has received clinical approval from the Food and Drug Administration (FDA) in 2018, which promotes the translation of gene therapy from concept to clinical utility.[44] Our results in this study indicated that the majority of *Pde3b* siRNA-loaded liposomes could be taken up by synovial macrophages in the inflamed joints, leading to reduced macrophage infiltration and enhanced anti-inflammatory program in the synovial tissues. As a consequence, administration of liposomes carrying the *Pde3b* siRNA significantly improved joint swelling, synovial inflammation, and bone erosion in CIA mice, and without the perceptible adverse effects. As tissue-infiltrating macrophages are the predominant macrophage population in RA synovium and positively correlated with the progress of inflammation and joint destruction,[10,13] we consider the decrease of macrophage proportion in synovial tissue may well be due to the reduction in tissue-infiltrating macrophages. We would tackle the effect of *Pde3b* knockdown on remodeling the resident or infiltrating macrophages in our future studies. Moreover, our human body have more intricate immune characteristics and internal environment as compared to mice. Therefore, there is still a long way to go before taking our findings into clinic.

Conclusions

In summary, the present study provides evidence that macrophages originating from arthritic mice are characterized by the higher levels of Pde3b. Silencing *Pde3b* significantly promotes macrophage anti-inflammatory program via cAMP-dependent PKA/CREB/C/EBPβ signaling. More importantly, administration of *Pde3b* siRNA-loaded liposomes significantly decreased Pde3b expression along with increased anti-inflammatory macrophage generation, thereby alleviating synovial inflammation and bone destruction following collagen induction. These findings broaden the current understanding of Pde3b in the regulation of macrophage polarization in pathological conditions, which may be informative in developing future medicine in clinical settings.

Data Sharing Statement

All data needed to evaluate the findings in this study are included in the manuscript and/or the Supplementary Information. Raw transcriptomic data have been deposited in the NCBI public repository Sequence Read Archive (Bioproject ID: PRJNA1025256, https://dataview.ncbi.nlm.nih.gov/object/PRJNA1025256?reviewer=5g2re1r4lpqegp5416eilve61p). Additional data related to this paper are available from the corresponding author upon request.

Acknowledgments

We thank Xin Wang, Yan Wang, and Yuan Sun from Institute of Hydrobiology, Chinese Academy of Sciences for technical assistance in micro-CT analysis and in vivo imaging system.

Funding

Our study was supported by the National Natural Science Foundation of China (82300929 and 82100892), Department of Science and Technology of Hubei Province Program Project (2022CFB739), the Intramural Research Program of the Central Hospital of Wuhan (21YJ01, 23YJ14), and Wuhan Talent Project.

Disclosure

The authors declare that they have no conflict of interest.

References

1. Biesemann N, Margerie D, Asbrand C, et al. Additive efficacy of a bispecific anti-TNF/IL-6 nanobody compound in translational models of rheumatoid arthritis. *Sci Transl Med*. 2023;15(681):eabq4419.
2. Yang Y, Guo L, Wang Z, et al. Targeted silver nanoparticles for rheumatoid arthritis therapy via macrophage apoptosis and Re-polarization. *Biomaterials*. 2021;264:120390.
3. Hoes JN, Jacobs JW, Buttgereit F, Bijlsma JW. Current view of glucocorticoid co-therapy with DMARDs in rheumatoid arthritis. *Nat Rev Rheumatol*. 2010;6(12):693–702.
4. Luo TT, Wu YJ, Yin Q, Chen WG, Zuo J. The Involvement of Glucose and Lipid Metabolism Alteration in Rheumatoid Arthritis and Its Clinical Implication. *J Inflamm Res*. 2023;16:1837–1852.
5. Liu D, Yuan N, Yu G, Song G, Chen Y. Can rheumatoid arthritis ever cease to exist: a review of various therapeutic modalities to maintain drug-free remission? *Am J Transl Res*. 2017;9(8):3758–3775.
6. Zhang S, Liu Y, Jing W, et al. Remodeling articular immune homeostasis with an efferocytosis-informed nanoimitator mitigates rheumatoid arthritis in mice. *Nat Commun*. 2023;14(1):817.
7. Galli SJ, Borregaard N, Wynn TA. Phenotypic and functional plasticity of cells of innate immunity: macrophages, mast cells and neutrophils. *Nat Immunol*. 2011;12(11):1035–1044.
8. Kang S, Nakanishi Y, Kioi Y, et al. Semaphorin 6D reverse signaling controls macrophage lipid metabolism and anti-inflammatory polarization. *Nat Immunol*. 2018;19(6):561–570.
9. Kim H, Back JH, Han G, et al. Extracellular vesicle-guided in situ reprogramming of synovial macrophages for the treatment of rheumatoid arthritis. *Biomaterials*. 2022;286:121578.
10. Cheng L, Wang Y, Wu R, et al. New Insights From Single-Cell Sequencing Data: synovial Fibroblasts and Synovial Macrophages in Rheumatoid Arthritis. *Front Immunol*. 2021;12:709178.
11. Smiljanovic B, Radzikowska A, Kuca-Warnawin E, et al. Monocyte alterations in rheumatoid arthritis are dominated by preterm release from bone marrow and prominent triggering in the joint. *Ann Rheum Dis*. 2018;77(2):300–308.
12. Alivernini S, MacDonald L, Elmesmari A, et al. Distinct synovial tissue macrophage subsets regulate inflammation and remission in rheumatoid arthritis. *Nat Med*. 2020;26(8):1295–1306.
13. Kurowska-Stolarska M, Alivernini S. Synovial tissue macrophages in joint homeostasis, rheumatoid arthritis and disease remission. *Nat Rev Rheumatol*. 2022;18(7):384–397.
14. Culemann S, Gruneboom A, Nicolas-Avila JA, et al. Locally renewing resident synovial macrophages provide a protective barrier for the joint. *Nature*. 2019;572(7771):670–675.
15. Movsesian M. Novel approaches to targeting PDE3 in cardiovascular disease. *Pharmacol Ther*. 2016;163:74–81.
16. Degerman E, Ahmad F, Chung YW, et al. From PDE3B to the regulation of energy homeostasis. *Curr Opin Pharmacol*. 2011;11(6):676–682.
17. Ahmad F, Degerman E, Manganiello VC. Cyclic nucleotide phosphodiesterase 3 signaling complexes. *Horm Metab Res*. 2012;44(10):776–785.
18. Zuo Y, Xu H, Li Y, Zhang Z, Tao R, Wang M. Hsa_circ_0007707 participates in PDE3B-mediated apoptosis inhibition and inflammation promotion in fibroblast-like synoviocytes. *Int Immunopharmacol*. 2023;119:110157.
19. Wang R, Sun Y, Jin X, Wen W, Cao Y. Diosgenin Inhibits Excessive Proliferation and Inflammatory Response of Synovial Fibroblasts in Rheumatoid Arthritis by Targeting PDE3B. *Inflammation*. 2021;44(3):946–955.
20. Leuschner F, Dutta P, Gorbatov R, et al. Therapeutic siRNA silencing in inflammatory monocytes in mice. *Nat Biotechnol*. 2011;29(11):1005–1010.
21. Chen Q, Gao M, Li Z, et al. Biodegradable nanoparticles decorated with different carbohydrates for efficient macrophage-targeted gene therapy. *J Control Release*. 2020;323:179–190.
22. Yan L, Hou C, Liu J, et al. Local administration of liposomal-based Plekhf1 gene therapy attenuates pulmonary fibrosis by modulating macrophage polarization. *Sci China Life Sci*. 2023.
23. Wang Y, Zhang L, Wu GR, et al. MBD2 serves as a viable target against pulmonary fibrosis by inhibiting macrophage M2 program. *Sci Adv*. 2021;7(1).
24. Wu GR, Zhou M, Wang Y, et al. Blockade of Mbd2 by siRNA-loaded liposomes protects mice against OVA-induced allergic airway inflammation via repressing M2 macrophage production. *Front Immunol*. 2022;13:930103.
25. Ngoune R, Contini C, Hoffmann MM, von Elverfeldt D, Winkler K, Putz G. Optimizing Antitumor Efficacy and Adverse Effects of Pegylated Liposomal Doxorubicin by Scheduled Plasmapheresis: impact of Timing and Dosing. *Curr Drug Deliv*. 2018;15(9):1261–1270.
26. Chen J, Chen J, Tan J, et al. HIF-1alpha dependent RhoA as a novel therapeutic target to regulate rheumatoid arthritis fibroblast-like synoviocytes migration in vitro and in vivo. *J Orthop Translat*. 2023;40:49–57.
27. Chen J, Tan J, Li J, et al. Genetically Engineered Biomimetic Nanoparticles for Targeted Delivery of mRNA to Treat Rheumatoid Arthritis. *Small Methods*. 2023;7(11):e2300678.
28. Chen J, Zeng S, Xue Q, et al. Photoacoustic image-guided biomimetic nanoparticles targeting rheumatoid arthritis. *Proc Natl Acad Sci U S A*. 2022;119(43):e2213373119.
29. Wang Z, Zhang C, Meng J, et al. A Targeted Exosome Therapeutic Confers Both Cfdna Scavenging and Macrophage Polarization for Ameliorating Rheumatoid Arthritis. *Adv Mater*. 2023;e2302503.

30. Deng C, Zhang Q, He P, et al. Targeted apoptosis of macrophages and osteoclasts in arthritic joints is effective against advanced inflammatory arthritis. *Nat Commun*. 2021;12(1):2174.
31. Chen L, Zhang J, Zou Y, et al. Kdm2a deficiency in macrophages enhances thermogenesis to protect mice against HFD-induced obesity by enhancing H3K36me2 at the Pparg locus. *Cell Death Differ*. 2021;28(6):1880–1899.
32. Yuan Q, Zhao B, Cao YH, et al. BCR-Associated Protein 31 Regulates Macrophages Polarization and Wound Healing Function via Early Growth Response 2/C/EBPbeta and IL-4Ralpha/C/EBPbeta Pathways. *J Immunol*. 2022;209(6):1059–1070.
33. Zhang H, Kong Q, Wang J, Jiang Y, Hua H. Complex roles of cAMP-PKA-CREB signaling in cancer. *Exp Hematol Oncol*. 2020;9(1):32.
34. Hsu CG, Fazal F, Rahman A, Berk BC, Yan C. Phosphodiesterase 10A Is a Key Mediator of Lung Inflammation. *J Immunol*. 2021;206 (12):3010–3020.
35. Page CP, Spina D. Selective PDE inhibitors as novel treatments for respiratory diseases. *Curr Opin Pharmacol*. 2012;12(3):275–286.
36. Movsesian M, Ahmad F, Hirsch E. Functions of PDE3 Isoforms in Cardiac Muscle. *J Cardiovasc Dev Dis*. 2018;5(1).
37. Wang Y, Han CC, Cui D, Li Y, Ma Y, Wei W. Is macrophage polarization important in rheumatoid arthritis? *Int Immunopharmacol*. 2017;50:345–352.
38. Peng Y, Zhou M, Yang H, et al. Regulatory Mechanism of M1/M2 Macrophage Polarization in the Development of Autoimmune Diseases. *Mediators Inflamm*. 2023;2023:8821610.
39. Liu PS, Wang H, Li X, et al. alpha-ketoglutarate orchestrates macrophage activation through metabolic and epigenetic reprogramming. *Nat Immunol*. 2017;18(9):985–994.
40. Maurice DH, Ke H, Ahmad F, Wang Y, Chung J, Manganiello VC. Advances in targeting cyclic nucleotide phosphodiesterases. *Nat Rev Drug Discov*. 2014;13(4):290–314.
41. Bolger GB. The PDE-Opathies: diverse Phenotypes Produced by a Functionally Related Multigene Family. *Trends Genet*. 2021;37(7):669–681.
42. Ruffell D, Mourkioti F, Gambardella A, et al. A CREB-C/EBPbeta cascade induces M2 macrophage-specific gene expression and promotes muscle injury repair. *Proc Natl Acad Sci U S A*. 2009;106(41):17475–17480.
43. Apparailly F, Jorgensen C. siRNA-based therapeutic approaches for rheumatic diseases. *Nat Rev Rheumatol*. 2013;9(1):56–62.
44. Kulkarni JA, Witzigmann D, Chen S, Cullis PR, van der Meel R. Lipid Nanoparticle Technology for Clinical Translation of siRNA Therapeutics. *Acc Chem Res*. 2019;52(9):2435–2444.